THE D_e (T, t) PLOT: A STRAIGHTFORWARD SELF-DIAGNOSE TOOL FOR post-IR IRSL DATING PROCEDURES

XIAO FU

Department of Earth Sciences, the University of Hong Kong, Pokfulam Road, Hong Kong, China

Abstract: This study presents a new self-diagnose method for the recently developed post-IR infra-red stimulated luminescence (pIRIR) dating protocols. This criterion studies the dependence of equivalent dose (D_e) on measurement-temperature (T) and time (t), by applying the D_e (t) analysis to the IRLS and pIRIR signals measured under different temperatures, and combines these D_e (t) plots into one, so-called the D_e (T, t) plot. The pattern of the D_e (T, t) plot is shown to be affected by anomalous fading, partial bleaching and non-bleachable signal. A D_e plateau can be achieved in the D_e (T, t) plot only when the effects of these factors are insignificant. Therefore, this plot can be used as a self-diagnose tool for the validity of pIRIR results. The D_e (T, t) analysis has been applied to four recently developed pIRIR protocols, using aeolian samples with different ages. The results show that this self-diagnose tool can be applied to different pIRIR protocols for validating the pIRIR dating results and evaluating the pIRIR measurement conditions.

Keywords: post-IR IRSL, measurement temperature and time, D_e plateau, self-diagnose criterion.

1. INTRODUCTION

Quartz and feldspar are commonly used paleodosimeters in optically stimulated luminescence (OSL) dating techniques. Over the past few years, feldspar infra-red stimulated luminescence (IRSL) dating has received much attention since the upper dating limit of feldspar is much higher than that of quartz OSL dating. However, the wide application of feldspar dating has been hampered by the anomalous fading phenomenon (Wintle, 1973; Spooner, 1994), which leads to underestimation for the feldspar dating results. It has been reported that in IRSL dating, the anomalous fading rate decreases with higher IR stimulation temperature or longer IR stimulation time (Thomsen *et al.*, 2008; Tsukamoto *et al.*, 2006). Based on the former, the post-IR IRSL (pIRIR) protocols

have been proposed that target the more stable signal from K-feldspar. These protocols include: 1) the two-step pIRIR dating protocol, which used an one-step lower temperature IR stimulation (at 50°C in Buylaert *et al.* (2009; 2012) and at 200°C in Li and Li (2011b)) to eliminate the easy-to-fade signals, then followed by an elevated temperature second-step IR stimulation (at 225°C in Buylaert *et al.* (2009); at 290°C in Thiel *et al.* (2011) and Buylaert *et al.* (2012)) to extract signals less affected by anomalous fading; and 2) the multi-elevated-temperature post-IR IRSL (MET-pIRIR) protocol, which utilizes multi-step IR stimulation at successively higher temperatures from 50 to 300°C to remove the fading signal progressively (Li and Li, 2011a; 2012). The upper dating limit of the MET-pIRIR methods is suggested to be up to ~300 ka (Li and Li, 2012), which is close to the saturation level of the pIRIR$_{250}$ and pIRIR$_{300}$ signals.

Corresponding author: X. Fu
e-mail: h1092075@hku.hk, xiaofuled@gmail.com

These newly developed methods have been tested using samples with independent age control. Many studies have reported that accurate dating results can be achieved for well-bleached samples (e.g. Buylaert *et al.*, 2012; Li and Li, 2011a, 2011b; 2012; Fu *et al.*, 2012a; Kars *et al.*, 2012). However, there were also examples showing that inaccurate age can be obtained if the measurement condition is inappropriate (e.g. Li and Li, 2011b; Roberts, 2012), or if the samples are poorly bleached (e.g. Lowick *et al.*, 2012). In this case, appropriate self-diagnose criteria are important to examine the dating results for these protocols, especially when independent chronological control is absent. In the MET-pIRIR dating protocol (Li and Li, 2011a), the dating results are shown as plots of age *vs.* IR stimulation temperature (the Age-T plots). Li and Li (2011a) suggested that if an age plateau can be reached in the Age-T plot at higher IR stimulation temperature, it represents that the non-fading signal has been obtained, and the effect of residual dose is negligible, or appropriately corrected for. Therefore, in the MET-pIRIR method, the Age-T plot can be used as a self-diagnose tool, and it can be obtained directly from the dating result. For the two-step pIRIR protocol, Roberts (2012) and Biswas *et al.* (2013) examined their measurement conditions using a plateau test by changing preheat and pIRIR stimulation temperatures. However, such test has to be conducted separately using different groups of aliquots. In this study, on the basis of the Age-T plot test of Li and Li (2011a), it is aimed at developing a new straightforward self-diagnose tool for different pIRIR protocols, which can be obtained directly from single-aliquot dating results, and can equally be applied to the different types of pIRIR dating protocols.

2. SAMPLES AND EQUIPMENTS

Samples used in this study are from the well-studied Luochuan section on the central Chinese Loess Plateau (e.g. Liu, 1985; Porter and An, 1995; Lu *et al.*, 2007; Lai, 2010). The chronology of the upper most layers S0 and L1 of the section has been established previously by Lu *et al.* (2007), Lai (2010) and Fu *et al.* (2012a), using quartz OSL dating. For the lower part of the section, the ages of the loess/paleosol boundaries can be obtained by climatic correlation to the well-established chronology in the marine sediments reported by Imbrie *et al.* (1984) (Liu, 1985; An *et al.*, 1991; Porter and An, 1995). In this study, the layer transition ages provided by Ding *et al.* (2002) is utilized to control the loess/paleosol boundaries. The quartz OSL dating results for the upper part of the Luochuan section showed that the sedimentation within L1 is continuous (Lu *et al.*, 2007; Lai, 2010; Fu *et al.*, 2012a). On the basis of paleomagnetic investigation of Chinese loess, Zhu *et al.* (2007) also suggested that loess sedimentation at the central and southern Loess Plateau (including the Luochuan section) during the last glaciation is continuous at the time scale of about 2 ka. Take the L1

layer as an analogue for older loess/paleosol layers, the deposition within a loess/paleosol layer is inferred to be continuous for the Luochuan section. Therefore, the ages of samples within a loess/paleosol layer can be estimated by linearly interpolating its sampling depth into the corresponding loess/paleosol boundary ages in which the samples were embedded.

Ten samples were collected within the upper 20 m of the section, from the Holocene soil unit S0 to the second paleosol layer S2. Samples LC-004, LC-035, LC-054 and LC-082 were collected from layers S0 and L1. Their quartz OSL ages, vary from 0.7 to 62 ka, are provided by Fu *et al.* (2012a). Samples LC-096, LC-120, LC-190 and LC-205 were collected from layers S1, L2 and S2. These samples were at or near the boundary of the loess/paleosol transition boundaries, so their ages are controlled by the boundary ages, from 75 to 214 ka. Samples LC-150 and LC-170 were collected within L2. Their expected ages (152 and 170 ka respectively) were obtained by linearly interpolating between boundary ages (Li and Li, 2012). All the feldspar MET-pIRIR ages and part of the two-step pIRIR ages for these samples have been published in previous studies (Fu *et al.*, 2012a; Li and Li, 2012; 2011b). For the youngest sample LC-004 (~0.7 ka), the MET-pIRIR age show overestimation when the non-bleachable dose is not corrected (Fu *et al.*, 2012a), but after the non-bleachable dose subtracted, the MET-pIRIR age is consistent with the quartz OSL age (section 4 in this study). For other samples, the feldspar dating results are consistent with the expected ages (Fu *et al.*, 2012a; Li and Li, 2012; 2011b), suggesting that these samples are well bleached. A summary of the samples used is given in **Table 1**.

All the samples were prepared using a routine separation technique (Aitken, 1998). The bulk samples were first treated with 10% HCl and 30% H_2O_2 to remove carbonates and organic matter, respectively. Then, grains of 63–90 μm were obtained by wet sieving. The K-feldspar extracts were separated by density separation using heavy liquid with a density of 2.58 g/cm³. These K-feldspar grains were then etched with 10% HF for 10 minutes to remove the α-dosed layer. The K-feldspar extracts were prepared for measurement by mounting on 9.8 mm diameter aluminum discs using "Silkospay" silicone oil. All luminescence measurements were performed using automated Risø TL/OSL-DA-15 or TL/OSL-DA-20 readers with $^{90}Sr/^{90}Y$ beta sources. IR measurements were performed using IR diodes (870Δ40 nm). Luminescence was detected by EMI 9235QA photomultiplier tube with a filter pack of Schott BG-39 and Corning 7–59 filters in front of the PMT (transmission range 320–480 nm). For all thermal treatments, a heating rate of 5°C/s was used. For the bleaching experiments, an ORIEL solar simulator was used. Dose rates for all the samples used are cited from previous studies (Fu *et al.*, 2012a; Li and Li, 2012, see **Table 1**).

Table 1. *A summary of sample depth, stratigraphic units, dose rates, ages and D$_e$ values for the samples.*

Sample	Depth (m)	Unit	KF dose rate (Gy/ka)[a]	Expected age (ka)[b]	Expected KF D$_e$ (Gy)[c]	Measured KF age (ka)[d]	Measured KF D$_e$ (Gy)[d]	Reference
LC-004	0.4	S0	3.7 ± 0.2	0.7 ± 0.1	2.6 ± 0.5	0.6 ± 0.1	2.2 ± 0.4	This study
LC-035	3.5	L1	3.6 ± 0.2	31 ± 4	110 ± 15	27.2 ± 1.7	98.0 ± 1.3	Fu et al., 2012a
LC-054	5.4	L1	3.7 ± 0.3	46 ± 4	168 ± 16	42.4 ± 2.8	154.2 ± 4.5	Fu et al., 2012a
LC-082	8.2	L1	3.5 ± 0.2	62 ± 7	215 ± 25	66.1 ± 3.9	229.4 ± 3.2	Fu et al., 2012a
LC-096	9.6	S1	3.7 ± 0.1	75 ± 5	273 ± 18	75.5 ± 3.7	276.3 ± 13.5	Li and Li, 2011b; 2012
LC-120	12	S1	3.5 ± 0.1	124 ± 5	425 ± 17	117.1 ± 14.3	405 ± 49	Li and Li, 2011b; 2012
LC-150	15	L2	3.4 ± 0.1	152 ± 10	512 ± 34	153 ± 16	514 ± 54	Li and Li, 2011b; 2012
LC-170	17	L2	3.6 ± 0.1	170 ± 10	612 ± 36	164 ± 10	584 ± 36	Li and Li, 2011b; 2012
LC-190	19	L2	3.6 ± 0.1	187 ± 10	660 ± 36	182 ± 18	648 ± 64	Li and Li, 2012
LC-205	20.5	S2	3.5 ± 0.1	214 ± 10	740 ± 35	223 ± 18	772 ± 62	Li and Li, 2011b; 2012

[a] *In external dose rate calculation, the contributions from U, Th were measured using the thick-source alpha counting technique (Aitken, 1985). The content of K was measured using X-ray fluorescence. Cosmic-ray dose rate was calculated following Prescott and Hutton (1994). In internal dose rate calculation, the internal K content was assumed to be $13 \pm 1\%$ (Zhao and Li, 2005) and the internal Rb content was assumed to be 400 ± 100 ppm (Huntley and Hancock, 2001).*

[b] *The expected ages for samples within S0 and L1 are based on coarse grain quartz OSL dating results (see Fu et al., 2012a). The expected ages for other samples are based on stratigraphic age control of Ding et al. (2002) (see Li and Li, 2012).*

[c] *The expected KF D$_e$ values are calculated using the expected ages and the measured dose rates.*

[d] *The measured KF ages and D$_e$ values for all the samples are based on coarse grain K-feldspar MET-pIRIR dating results (see Fu et al., 2012a and Li and Li, 2012). For the youngest sample LC-004, non-bleachable dose has been corrected; for other samples, non-bleachable dose is not corrected since it is negligible compared with the natural dose (see section 4).*

3. D_e AS A FUNCTION OF MEASUREMENT TEMPERATURE AND TIME

Previous studies showed that the anomalous fading rate decreases as a function of increasing IR stimulation temperature (T), as well as a function of measurement time (t) (Thomsen *et al.*, 2008; Tsukamoto *et al.*, 2006). The Age-T (or D_e-T) plot in the MET-pIRIR protocol of Li and Li (2011a; 2012) only investigate the dependence of age (or D_e) on IR stimulation temperature, while the plateau was typically detected at 2–3 IR stimulation temperatures. A further investigation of the dependence of age (or D_e) on IR stimulation time in pIRIR protocols will help providing a more detailed picture about the change of age (or D_e). The measurement-time dependence of D_e can be investigated using the D_e (t) plot (Huntley *et al.*, 1985; Bailey, 2000). Here, the D_e-T plot (Li and Li, 2011a) and the D_e (t) plot are investigated together, in order to develop a new self-diagnose criterion for the pIRIR methods, the so called D_e (T, t) plot.

An example of the D_e (T, t) plot for the MET-pIRIR method (Li and Li, 2011a, see detailed procedures in **Table 2**) is given in **Fig. 1**, using sample LC-054. The natural decay curves of the MET-pIRIR signals are shown in **Fig. 1**. Five IRSL/pIRIR decay curves are obtained corresponding to different IR stimulation temperatures. To construct the D_e (T, t) plot, D_e (t) analysis was first applied separately to IRSL and MET-pIRIR signals obtained under different T. In the D_e (t) plots for each signal (with 100 s IR stimulation), the time-interval for each integration was selected to be 5 s, and the increment
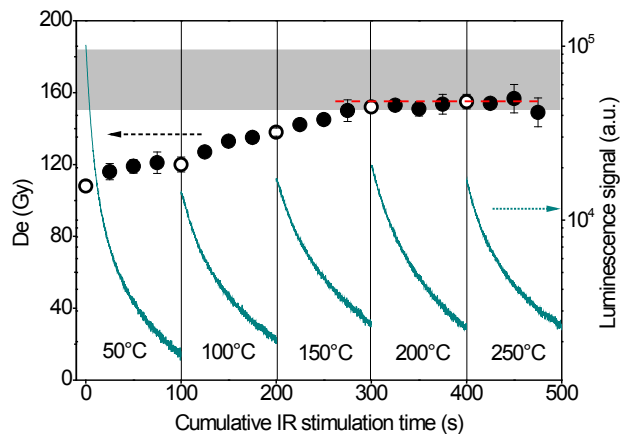
Fig. 1. D$_e$ *of sample LC-054 obtained using the MET-pIRIR method (Table 2) plotted against the cumulative IR stimulation time (t). For each measurement step, the measure duration is 100 s, and there is an increase in IR stimulation temperature (T) of 50°C between steps. The open circles represent D$_e$ corresponding to the initial signal (D$_{e-is}$) for each step. The D$_e$ plateau is shown as dash line. The gray belt represents the expected D$_e$. Each data point represents the mean of 8 aliquots, and error bars show the 1 sigma standard error. The natural decay curves of the MET-pIRIR signals are also given.*

between adjacent time intervals was arbitrary chosen to be 25 s (e.g., the integration intervals of IRSL signal at 50°C are 0–5, 25–30, 50–55 and 75–80 s). The background subtracted for each integration interval is estimated from the mean count rate of the last 5 s for the corresponding IRSL or pIRIR signal. Then, these D_e (t) plots

Table 2. *Summary of the measurement protocols.*

Step	MET-pIRIR[a]	Three-step pIRIR	Two-step pIRIR (50, 290)	Two-step pIRIR (200, 290)
1	Give regenerative dose, D_i	Give regenerative dose, D_i	Give regenerative dose, D_i	Give regenerative dose, D_i
2	Preheat at 300°C for 10 s	Preheat at 300°C for 10 s	Preheat at 320°C for 60 s	Preheat at 320°C for 60 s
3	IRSL at 50°C for 100 s, $L_{x(50)}$	IRSL at 150°C for 100 s, $L_{x(150)}$	IRSL at 50°C for 200 s, $L_{x(50)}$	IRSL at 200°C for 200 s, $L_{x(200)}$
4	IRSL at 100°C for 100 s, $L_{x(100)}$	IRSL at 200°C for 100 s, $L_{x(200)}$	IRSL at 290°C for 200 s, $L_{x(290)}$	IRSL at 290°C for 200 s, $L_{x(290)}$
5	IRSL at 150°C for 100 s, $L_{x(150)}$	IRSL at 250°C for 100 s, $L_{x(250)}$	Give test dose, D_t	Give test dose, D_t
6	IRSL at 200°C for 100 s, $L_{x(200)}$	Give test dose, D_t	Preheat at 320°C for 60 s	Preheat at 320°C for 60 s
7	IRSL at 250°C for 100 s, $L_{x(250)}$	Preheat at 300°C for 10 s	IRSL at 50°C for 200 s, $L_{x(50)}$	IRSL at 200°C for 200 s, $L_{x(200)}$
8	Give test dose, D_t	IRSL at 150°C for 100 s, $T_{x(150)}$	IRSL at 290°C for 200 s, $L_{x(290)}$	IRSL at 290°C for 200 s, $L_{x(290)}$
9	Preheat at 300°C for 10 s	IRSL at 200°C for 100 s, $T_{x(200)}$	IR bleaching at 325°C for 40 s	IR bleaching at 325°C for 40 s
10	IRSL at 50°C for 100 s, $T_{x(50)}$	IRSL at 250°C for 100 s, $T_{x(250)}$	Return to step 1	Return to step 1
11	IRSL at 100°C for 100 s, $T_{x(100)}$	IR bleaching at 320°C for 100 s		
12	IRSL at 150°C for 100 s, $T_{x(150)}$	Return to step 1		
13	IRSL at 200°C for 100 s, $T_{x(200)}$			
14	IRSL at 250°C for 100 s, $T_{x(250)}$			
15	IR bleaching at 320°C for 100 s			
	Return to step 1			

[a] In the MET-pIRIR method, an additional measurement step of pIRIR at 300°C for 100 s can be added after the 250°C pIRIR measurements (steps 7 and 14) for samples older than 100 ka to achieve a plateau in the age-T plot. Correspondingly, the preheating condition is changed to be at 320°C for 60 s, and the IR bleaching at the end of each cycle is conducted at 325°C (see Li and Li, 2012).

Note: For all protocols, before the IRSL or pIRIR stimualtion, aliquots were held at the measurement temperature for 5 s without IR stimulation to eliminate the influence of isothermal TL (Fu et al., 2012a; Wang and Wintle, 2013).

are connected using a cumulative IR stimulation time t to give the D_e (T, t) plot (**Fig. 1**). Three points about this plot should be noted: first, the D_e values obtained from the initial part of each signal ($D_{e\text{-is}}$, the open circles in **Fig. 1**) are the routinely used D_e values for the D_e-T plot in the MET-pIRIR method. So, the D_e (T, t) plot include the D_e-T plot; second, the time axis in the D_e (T, t) plot is the accumulated IR stimulation time from different signals, rather than the real IR stimulation time for each measurement step; third, to depict the D_e (T, t) plot more directly, in this paper I mainly refer to the value of the cumulative time t when describing the D_e (T, t) plot. It should be kept in mind, however, that for each step of pIRIR stimulation, there is an increase of IR stimulation temperature (which plays significant role in reducing anomalous fading). Therefore, the D_e (T, t) plot is a three-dimensional plot reflects a combined effect of T and t on the value of D_e.

The result in **Fig. 1** shows that D_e value is a function of both T and t. The most significant underestimation in D_e is observed in the first data point. Then, a gradual increasing in D_e when the cumulative t increases from 0 to 300 s is observed, with the fading component gradually removed. After that, a plateau in D_e is reached after 300 s. The achievement of a plateau in the D_e-T test was used by Li and Li (2011a) to judge whether the non-fading signal has been obtained. Comparison between the D_e plateau obtained in **Fig. 1** with the expected D_e (the grey belt) for the sample show that they consist well, indicating the achievement of non-fading signal. This suggests that the D_e (T, t) plot can also be serviced as such a self-judge as the D_e-T plot. Compared with the D_e-T plot (the open

circles in **Fig. 1**), the advantage of using the D_e (T, t) plot analysis is that it provides more data points about the change of D_e, and therefore the D_e plateau can be obtained more reliably. Besides, it is expected that the D_e (T, t) plot can also be applied to procedures with fewer measurement steps (e.g. two-step pIRIR protocols), since it is less limited by the temperature treatment given.

4. FACTORS AFFECTING THE D_e (T, t) PLOT

D_e value in pIRIR protocol is potentially affected by factors such as anomalous fading (e.g. Thomsen *et al.*, 2008; Li and Li, 2011a), partial bleaching (e.g. Lowick *et al.*, 2012) and non-bleachable signal (e.g. Buylaert *et al.*, 2011; Stevens *et al.*, 2011; Li *et al.*, 2013), etc. Here, the MET-pIRIR method is taken as an example to study the effects of different factors on the D_e (T, t) plot. Most of the experiments were carried out on a Holocene sample LC-004 (expected D_e 2.6 ± 0.5 Gy).

Dose recovery test

A dose recovery experiment (Wallinga *et al.*, 2000) was first carried out to confirm the measurement procedures, and designed to show a D_e (T, t) plot that is not mainly affected by the above factors. In the experiment, 4 natural aliquots of sample LC-004 were given a β dose of 260 Gy; this dose was treated as unknown dose, and measured immediately using the MET-pIRIR protocol (**Table 2**) after irradiation (test dose = 130 Gy). The immediate measurement after irradiation minimizes the effect of anomalous fading. The natural dose of the sam-

ple is ~2–6 Gy for the IRSL and MET-pIRIR signals (see **Fig. 3**), which is only less than 3% of the given dose. This natural dose was subtracted from the final result to correct the residual dose before the irradiation. The non-bleachable doses (~1–4 Gy, see **Fig. 3**) are insignificant compared with the given dose. So, the effect of non-bleachable dose should also be very limited in the final result.

The D_e (T, t) plot for the dose recovery experiment is given in **Fig. 2**. It is shown that in the D_e (T, t) plot a plateau consistent with the given dose is obtained. The measured D_e values are within 1.0 ± 0.1 of the given dose for all integration intervals. This result is interesting compared with some previous reports, e.g., Li and Li (2011a) and Fu and Li (2013) all observed that pIRIR signals give better dose recovery results than IRSL signal in the MET-pIRIR method. Dose recovery result can be affected by various factors, such as what sample is used (bleached or modern/young sample) or the size of test dose (e.g. Qin and Zhou, 2012). Although this is not within the scope of this study, it deserves further research in the future. The dose recovery result in **Fig. 2** confirms the MET-pIRIR protocol listed in **Table 2**. It also indicates that in the MET-pIRIR protocol, if the effects of factors such as anomalous fading, partial bleaching and non-bleachable dose are negligible, a flat D_e (T, t) plot should be observed. The D_e plateau in the plot should be consistent with the true D_e value.

Effect of the non-bleachable signals on D_e (T, t) plot

Non-bleachable signals in IRSL and pIRIR signals are defined as signals which can hardly be bleached by sunlight, *i.e.*, the remnant signal observed in fully sunlight-
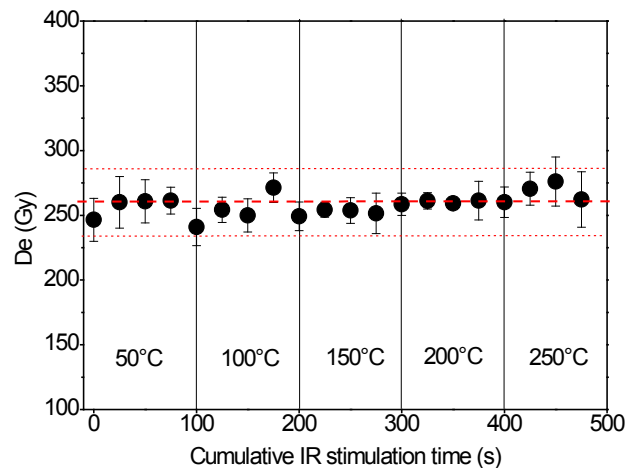

Fig. 2. D_e *(T, t) plot of dose recovery result for the MET-pIRIR method (Table 2), using sample LC-004 (see experimental details in text). The given dose for recovery is 260 Gy (shown as dash lines). The dotted lines show 1.0 ± 0.1 of the given dose. The natural dose has been subtracted. Each data point represents the mean of 4 aliquots, and error bars show the 1 sigma standard error.*

bleached samples. To determine an appropriate solar bleaching duration to detect the non-bleachable signal, 6 groups of aliquots of sample LC-004 (3 aliquots for each) were bleached for different durations up to 8 hours using a solar simulator, and then measured using the MET-pIRIR protocol in **Table 2**. The residual signals (defined as the remained signal after a certain time of solar bleaching) for different groups are shown in **Fig. 3a**. As expected, a signal obtained at higher temperature is harder to bleach (as e.g. Li and Li, 2011a; Buylaert *et al.*, 2011; Fu *et al.*, 2012b). The result shows that when the solar bleaching time exceeds 4 hours, all IRSL and pIRIR signals show no longer obvious reduction. Similar result was observed for other samples in **Table 1**. Therefore, the residual signals after solar bleaching for 4 hours are considered to be non-bleachable for samples in this study. **Fig. 3a** shows that the non-bleachable components accounts for a high proportion of the natural IRSL and pIRIR signals for sample LC-004, vary from ~30% for the $IRSL_{50}$ signal to ~70% for the MET-pIRIR$_{250}$ signal. It indicates that the non-bleachable signal should have an obvious effect on the dating result of this young sample.

To study the effect of thermal transfer on non-bleachable dose and it potential influence on the D_e (T, t) plot, non-bleachable doses of sample LC-004 were measured using MET-pIRIR protocols with varied preheating temperatures at 300, 320 and 340°C (preheating time was 10 s). The D_e (T, t) plots obtained are given in **Fig. 3b**. For all the preheating temperatures, the D_e value keeps increasing in the entire D_e (T, t) plot. For example, for the 300°C preheating, the non-bleachable dose gradually changes from 0.8 to 4.2 Gy, from the initial to the later part of the plot. This indicates that the non-bleachable dose increases with both T and t. Besides that, the residual doses also increase with higher preheating temperature. The highest dose (the last data point) for the 300 and 340°C preheating are 4.2 and 5.9 Gy, respectively. This suggests that thermal transfer plays a significant part in the non-bleachable signal (consistent with e.g. Buylaert *et al.*, 2011; Fu and Li, 2013). The influence of non-bleachable signal becomes larger for more stringent pre-heating.

The natural dose of sample LC-004 has also been measured with different preheat temperatures as in **Fig. 3b**, and the obtained D_e (T, t) plots are given in **Fig 3c**. Increasing D_e (T, t) with no plateau was observed for all the measurements, while higher D_e values were obtained for higher preheat temperatures. Compared with the expected D_e (the gray belt), all the pIRIR D_e values are shown to be overestimated. In **Fig. 3d**, the data in **Fig. 3c** are corrected for the non-bleachable dose using data from **Fig. 3b**. After correction, all D_e values are consistent with the expected D_e with error after 200 s ($T = 150°C$), for all the preheating temperatures. This further confirms that the overestimation of the D_e is caused by non-bleachable signal for this sample. The results of **Fig. 3** imply that non-bleachable signal can cause raised D_e (T, t) for young
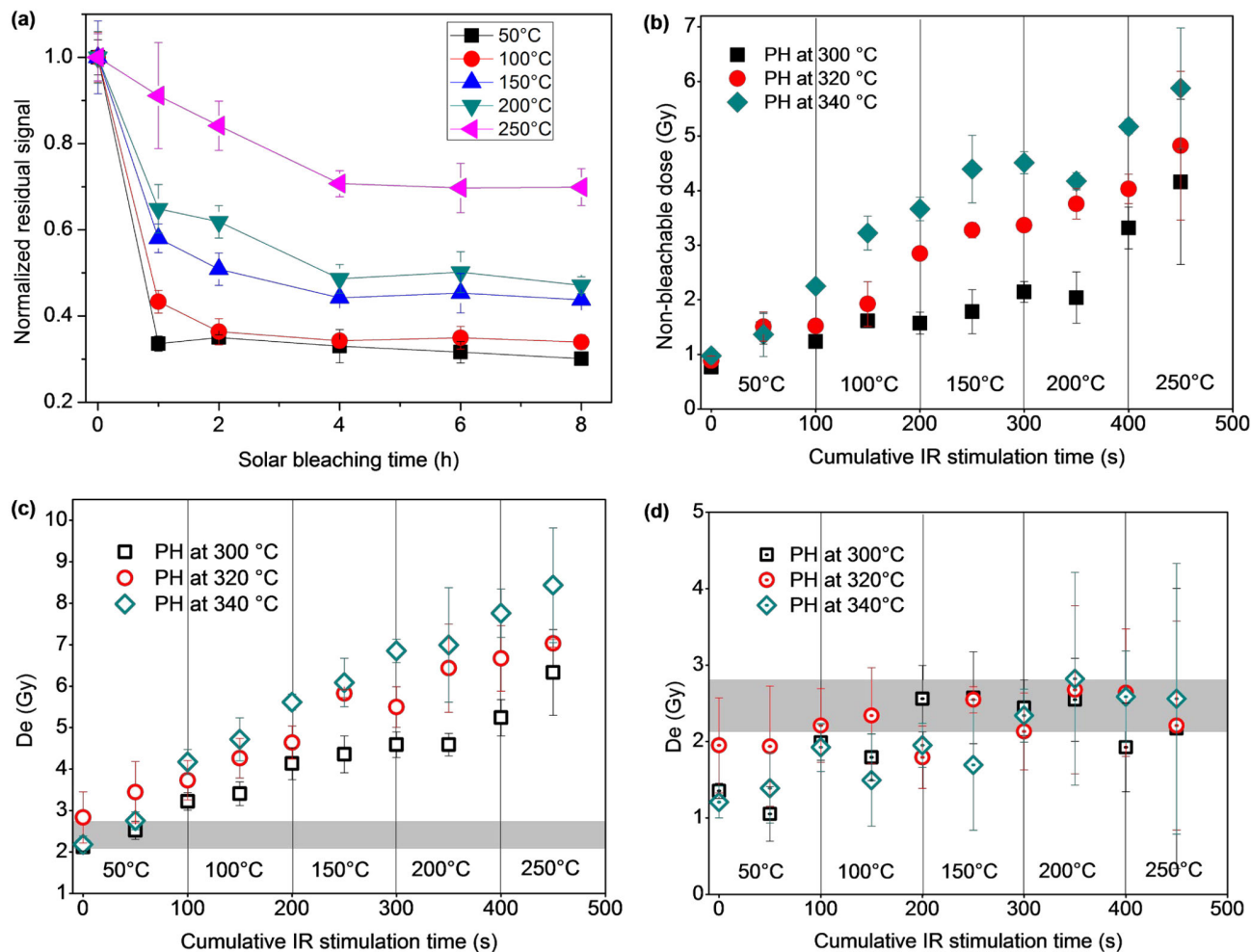
Fig. 3. *a) Residual signal of sample LC-004 plotted against solar bleaching time. All data are normalized to the unbleached natural signals. b) Non-bleachable dose of sample LC-004 obtained with different preheating temperatures plotted against cumulative IR stimulation time (t). Aliquots after 4 hours solar bleaching were used. c) D_e (T, t) plots for sample LC-004 obtained with different preheating temperatures. d) Data from c) are corrected for non-bleachable dose using data from b). The gray belt represents expected D_e. It is noted that a time increment of 50 s between the adjacent time intervals is used for data in this figure. Each data point represents the mean of 4 aliquots, and error bars show the 1 sigma standard error.*

samples. A plateau in the D_e (T, t) plot can be obtained when the effect of non-bleaching dose is appropriately corrected. The non-bleachable dose for other older samples in **Table 1** has also been measured. It is found that the non-bleachable doses for these samples are all within ~0.5–5 Gy for the IRSL and pIRIR signals (comparable to e.g. Li and Li., 2011a, Fu *et al.*, 2012a and Buylaert *et al.*, 2012). Therefore, for old samples, when the natural dose is significantly larger, the non-bleachable dose is not a major factor influencing the D_e (T, t) plot. The effect of non-bleachable dose can also be minimized using lower preheat and pIRIR stimulation temperatures (e.g. Madsen *et al.*, 2011; Reimann *et al.*, 2011; Reimann and Tsukamoto, 2012; Fu and Li, 2013). The D_e (T, t) plot can also be applied to these modified methods for self-diagnose.

Effect of partial bleaching on D_e (T, t) plot

The effect of insufficient signal resetting was studied using artificially dosed aliquots of sample LC-004. In the experiment, 12 aliquots of sample LC-004 were first given a β irradiation of 260 Gy, which is much larger than the natural dose of the sample (~2–6 Gy), similar as in the dose recovery test (**Fig. 2**). After irradiation, the aliquots were divided into three groups (4 aliquots each): in Group 1, the β dosed aliquots were first bleached for 20 s under the solar simulator, then immediately measured using the MET-pIRIR protocol in **Table 2**; in Group 2, the bleaching time before measurement was extended to be 60 s. In Group 3, after the solar bleaching of 20 s, an additional β dose of 26 Gy was added to the aliquots before MET-pIRIR measurement. The natural dose of the sample has been corrected in the final result obtained. The results got from the three groups are shown in **Fig. 4**.

Since the delay between irradiation and measurement was very short (20 and 60 s for Group 1 and 2, and ~220 s for Groups 3), and the non-bleachable dose is negligible compared with the given dose (**Fig. 3b**), anomalous fading and non-bleachable signal should not be the main factor affecting the results. The bleaching times for the three groups have been shown to be far from enough to fully reset the bleachable signals (**Fig. 3a**). Thus, partial bleaching should be the main factor influencing the results obtained.

In **Fig. 4a**, the ratio between the sensitivity corrected luminescence signal of Group 1 to that of the dose recovery test without bleaching (data for **Fig. 2a**) is plotted against T and t. This ratio represents the percentage of signal that remains after 20 s solar bleaching, and it can be used to show the variance in bleachability. The increasing tendency of the ratio is obvious in the figure: for initial part of the IRSL signal measured at 50°C ($t = 0$ s), less than 10% signals were remained after the bleaching; while with T and t increasing, this percentage raised gradually up to more than 40% ($t > 400$ s). This shows that the IRSL and pIRIR signals become harder to bleach from the beginning to the later part of the D_e (T, t) plot. In **Fig. 4b**, D_e (T, t) plots of the three groups are shown. All of the three groups show a continuous rise in D_e (T, t) plot, the higher D_e values in the later part of the D_e (T, t) plot indicate higher residual dose. No plateau in D_e is detected in the results. This indicates that significant partial bleaching will lead to a steady rising trend in the D_e (T, t) plot, and such an effect can be preserved after post-bleaching irradiation. In **Fig. 4c**, D_e values are normalized to the first point for each group to show the relative increase. The D_e values for the last point in the D_e (T, t) plots are shown to be ~7, 9 and 3 times larger than that of the first point for Group 1, 2 and 3, respectively. The relative increase of D_e with T and t for Group 2 is greater than Group 1. This further confirms that signals in the earlier part of the D_e (T, t) plot bleach faster than the later part (as shown in **Fig. 4a**). Comparison between Group 1 and 3 suggests that the post-bleaching irradiation can cause a smaller relative rise in the D_e (T, t) plot.

The results in **Fig. 4** imply that a rising D_e (T, t) plot without plateau may indicate significant partial bleaching. However, it should be noted that for natural samples, the fading effect can also cause increasing tendency in the D_e (T, t) plot (as shown in the next section), and the effects of the two factors can be mixed to make the problem more complex. One potential way of identifying the partial bleaching problem is to use the relative increase of D_e within the D_e (T, t) plot, as shown in **Fig. 4c**, for evaluation. For example, on the basis of the measured fading rate, one can estimate the relative increase of the D_e (T, t) plot for a well bleached sample with a certain age, and compare it with the measured D_e (T, t) plot to evaluate the possibility of partial bleaching. One can also combine the D_e (T, t) plot with D_e distribution characters to further confirm the existence of partial bleaching.
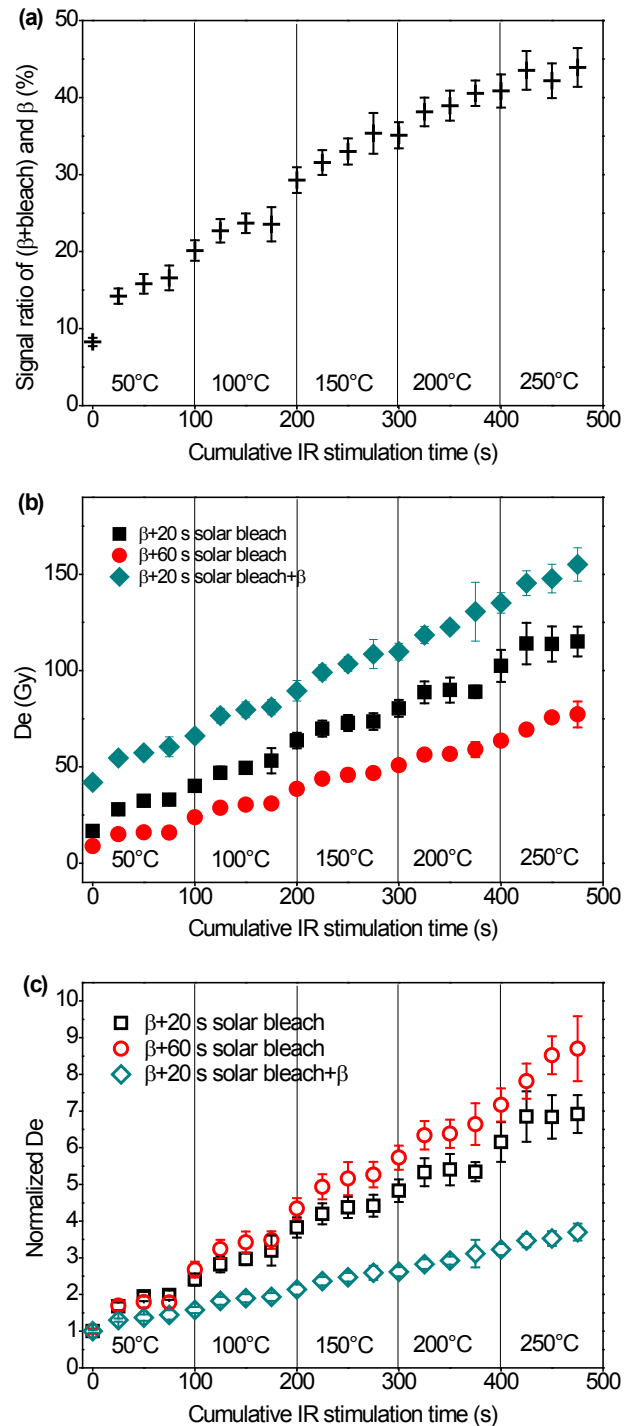

Fig. 4. *a) The ratio of the sensitivity corrected luminescence signal of sample LC-004 obtained from Group 1 (260 Gy β irradiation +20 s solar bleach) to that of the dose recovery test (260 Gy β irradiation +no bleach), plotted as a function of cumulative IR stimulation time (t). b) D$_e$ (T, t) plots for Group 1, Group 2 (260 Gy β irradiation +60 s solar bleach) and Group 3 (260 Gy β irradiation +20 s solar bleach +26 Gy β irradiation). c) D$_e$ (T, t) plots of the three groups in b) normalized to the first points. See measurement details in the text. Each data point in the plots represents the mean of 4 aliquots, and error bars show the 1 sigma standard error.*

Effect of anomalous fading on D_e (*T*, *t*) plot

For well-bleached old samples (to which the effects of non-bleachable signal and partial bleaching are negligible), anomalous fading has become the main factor influencing the D_e (*T*, *t*) plots. Anomalous fading rate is suggested to decrease with *t* (Tsukamoto *et al.*, 2006) and *T* (Thomsen *et al.*, 2008). The change in the anomalous fading rate (g-value (Aitken, 1985)) with *T* and *t* for MET-pIRIR signals of sample LC-004 is summarized in **Fig. 5a**. Here the g-value is measured according to Auclair *et al.* (2003), but using the MET-pIRIR procedure shown in **Table 2**. A g_{2days} of ~3.8%/decade was obtained at the beginning of the D_e (*T*, *t*). Then the g-value reduces with increasing *T* and *t*, and decreases to be lower than 1%/decade when *t* is 300 s or longer (at *T* is 200°C or higher). To further show the effect of anomalous fading on the D_e (*T*, *t*) plot, two groups of 4 aliquots of sample LC-004 were given a radiation dose of 260 Gy (similar to **Fig. 2**), and measured using the MET-pIRIR protocol (**Table 2**) after a delay of 6 and 15 days, respectively. After subtracting the natural dose, the results are compared with that of the dose recovery test with no delay (**Fig. 2**) in **Fig. 5b**. At the earlier part of the D_e (*T*, *t*) plots, underestimation is observed for the two groups with delay due to the fading effect, compared with the given dose and the D_e (*T*, *t*) plot for the dose recovery test. Larger underestimation is observed for the group with a longer delay, due to a larger signal loss induced by longer time for fading. For the group with a delay of 6 days, the D_e (*T*, *t*) plot reaches a plateau consistent with the given dose at *t* = 175 s (*T* = 100°C), while for the other group with a delay of 15 days, the plateau begins at *t* = 250 s (*T* = 150°C). This result suggests that in the D_e (*T*, *t*) plot, an age plateau should be obtained when the non-fading signal has been achieved. The age plateau should be achieved later in the D_e (*T*, *t*) plot for older samples compared with younger samples (as in **Fig. 5b**), because the signal related to the later part of the D_e (*T*, *t*) plot is more stable (as in **Fig. 5a**). Hence, the D_e (*T*, *t*) plot can be used to judge which signal should be chosen for dating, for samples with different ages.

5. APPLYING THE D_e (*T*, *t*) PLOT ANALYSIS TO VARIOUS post-IR IRSL DATING PROTOCOLS

As discussed above, the advantage of the D_e (*T*, *t*) plot is that it can use more data points for the D_e plateau detection. Therefore, it is expected that this tool should not only be applicable to the MET-pIRIR method, but also to other pIRIR dating protocols with fewer steps. The principles underlying the pIRIR protocols are the same, therefore, influencing factors (as shown in Section 4) on the D_e (*T*, *t*) plots for these methods should also be similar. In this section, the D_e (*T*, *t*) analysis is applied to four pIRIR dating methods, using samples from Luochuan (**Table 1**): 1) the MET-pIRIR method (Li and Li, 2011a; 2012), as in **Fig. 1**; 2) a simplified MET-pIRIR protocol with three
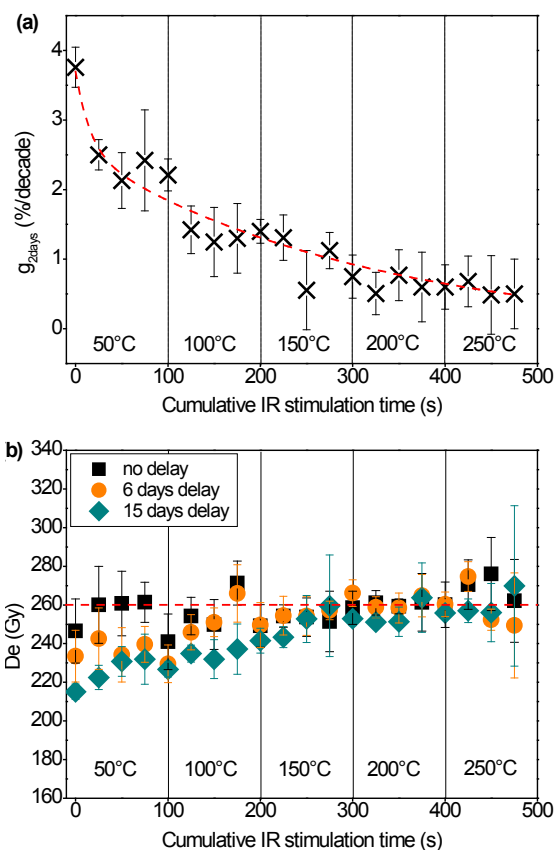
Fig. 5. *a) g-values (for the normalization time* t_c = *2 days) of the MET-pIRIR signals of sample LC-004 plotted against cumulative IR stimulation time (*t*). The dash line is the trend line fitted using two exponential decays. b)* D_e *(*T*, *t*) plots for three groups of aliquots of sample LC-004 given 260 Gy β irradiation, and measured after a delay of 0 s, 6 days and 15 days, respectively. The dash line represents the given dose. The natural dose has been subtracted. Each data point represents the mean of 4 aliquots, and error bars show the 1 sigma standard error.*

steps of IR stimulation at 150, 200 and 250°C; 3) the two-step pIRIR (50, 290) method (Thiel *et al.*, 2011; Buylaert *et al.*, 2012); 4) the two-step pIRIR (200, 290) method (Li and Li, 2011b). Detailed measurement procedures for these protocols are summarized in **Table 2**. The integration interval and background selection for all D_e (*T*, *t*) plots is similar as in **Fig. 1**. Dose recovery test similar as in section 4, has also been applied to the later three protocols. For all these methods, constant D_e (*T*, *t*) consistent with the given dose can be observed, similar to **Fig. 2**. Considering that these samples used are well-bleached aeolian samples (as shown in previous dating results (Fu *et al.*, 2012a; Li and Li, 2011b, 2012), and are old enough (except for sample LC-004) so the non-bleachable dose can be ignored (section 4 and **Fig. 3**), the effect of fading is the main factor controlling the pattern of the D_e (*T*, *t*)

plots for these samples. Examples shown in **Fig. 6** illustrate the use of D_e (T, t) analysis for the four pIRIR methods, using two typical samples: a younger sample LC-035 (~100 Gy) and an older sample LC-190 (~650 Gy). The routinely used D_e values ($D_{e\text{-is}}$) for the different pIRIR methods are shown as open circles or open diamonds to differentiate from other points. The expected D_e values are shown as gray belts.

Fig. 6a and **6d** presents the D_e (T, t) plots for the MET-pIRIR protocol for the two samples. For the younger sample LC-035 (**Fig. 6a**), it is observed that the D_e value increase with both T and t from 0 to 250 s in t, with the fading component gradually removed. The age plateau consistent with the expected D_e has been achieved at $t = 250$ s ($T = 150°C$), suggesting that non-fading signal has been reached at this point. The $D_{e\text{-is}}$ values for 200 and 250°C are identical and lie within the plateau. This suggests that for this sample, it is enough to use the conventional D_e-T plot (Li and Li, 2011a) for self-diagnose, and the D_e (T, t) plot can be used to more accurately confirming the plateau position. However, this is not always the case for older samples. For the older sample LC-190 (**Fig. 6d**), the original five-step MET-pIRIR protocol (Li and Li, 2011a) detects no plateau in D_e-T plot, since the $D_{e\text{-is}}$ value (open symbols) increases steadily from 50 to 250°C. After the D_e (T, t) analysis, a plateau consistent with the expected D_e can be detected, which starts at 400 s in t ($T = 250°C$), indicating that D_e values in this

range, e.g. the $D_{e\text{-is}}$ for 250°C, are reliable. Li and Li (2012) has proposed another six-step MET-pIRIR protocol, with an additional 300°C pIRIR step, for old samples. This protocol has also been applied to sample LC-190, and the obtained D_e (T, t) plot is also shown in **Fig. 6d**. A plateau in D_e has been reached at $t = 400$ s in the D_e (T, t) plot for this method ($D_{e\text{-is}}$ for 250 and 300°C are within the plateau). The D_e plateaus for the five-step and six-step MET-pIRIR methods are found to be consistent. Hence, for older samples, one can still apply the five-step MET-pIRIR protocol, with the help of the D_e (T, t) plot for plateau detecting. Compared with the six-step MET-pIRIR protocol, the five-step MET-pIRIR protocol can save measurement time, and avoid stronger thermal transfer introduced by more stringent preheating.

The D_e (T, t) analysis has also been applied to a further simplified MET-pIRIR method with three steps (**Table 2**), as shown in **Figs. 6b** and **6e**, for samples LC-035 and LC-190. Age plateaus consistent with the expected D_e are found to begin at $t = 125$ s ($T = 200°C$) and $t = 175$ s ($T = 200°C$) for the two samples, respectively. The plateaus are also consistent with that of the MET-pIRIR method (**Figs. 6a** and **6d**). These data demonstrate that the three-step pIRIR protocol is as effective as the MET-pIRIR protocol when using the D_e (T, t) plot to identify a plateau, *i.e.*, the D_e (T, t) plot can help further simplify the measurement procedure for the multi-step pIRIR protocol.
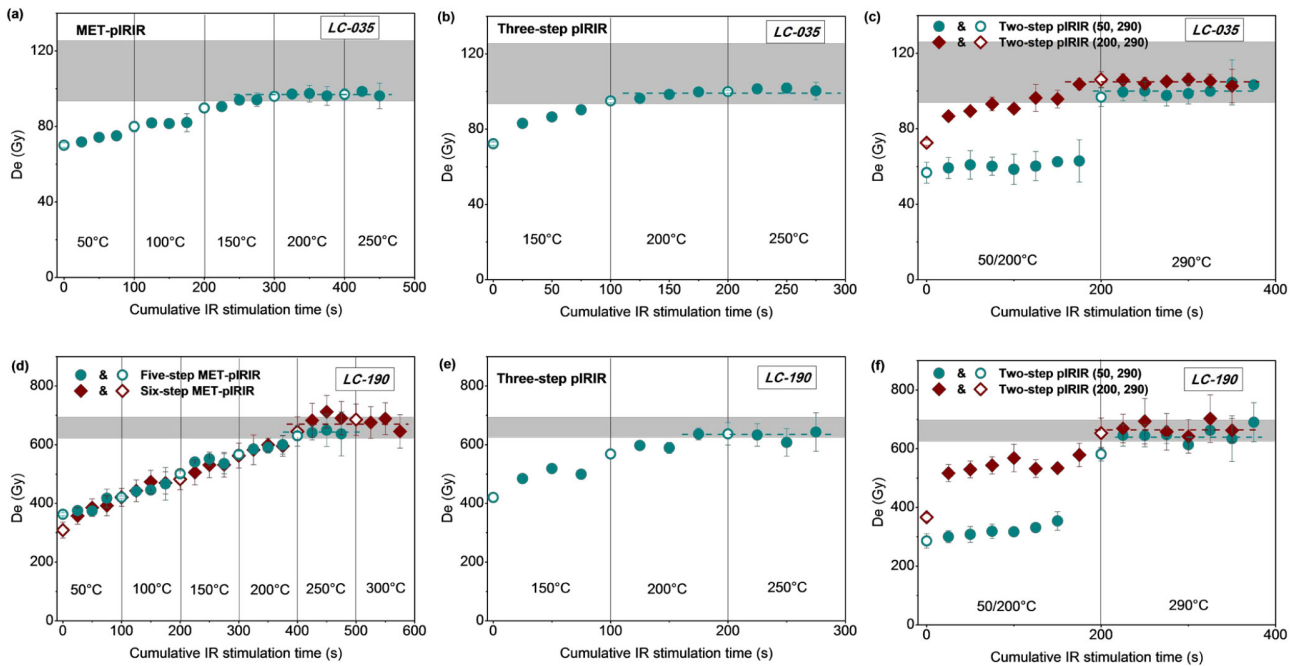

Fig. 6. D_e *(T, t) plots for samples LC-035 and LC-190 obtained using: a) and d) the MET-pIRIR method; b) and e) the three-step pIRIR method; c) and f) the two-step pIRIR (50, 290) and (200, 290) methods. See detailed measurement procedures in* Table 2. *The gray belts are the expected* D_e *values. The dash line represents the* D_e *plateau. The open circles or diamonds represent the* D_e *of the initial signal (*$D_{e\text{-is}}$*) for each step. Each data point in the plots represents the mean of 5–10 aliquots, and error bars show the 1 sigma standard error. It is noted that for the later part of some IRSL or pIRIR signal, due to low signal intensity, no* D_e *value can be obtained (e.g. at* t = 175 *s for the pIRIR (50, 290) protocol in f).*

In **Figs. 6c** and **6f**, the D_e (T, t) method is applied to the two-step pIRIR dating results for samples LC-035 and LC-190. For the younger sample LC-035 (**Fig. 6c**), the D_e plateaus consistent with the expected D_e start at 200 s ($T = 290°C$) and 175 s ($T = 200°C$) in t for the pIRIR (50, 290) and pIRIR (200, 290) methods, respectively. The plateau regions are consistent with each other for the pIRIR (50, 290) and pIRIR (200, 290) protocols (similar for **Fig. 6f**), and agree well with that of the MET-pIRIR protocols (**Figs. 6a** and **6b**). The $D_{e\text{-is}}$ values of 290°C (the open circle and diamond at $t = 200$ s) for the two methods are all within the plateaus, indicating that the pIRIR$_{290}$ $D_{e\text{-is}}$ values of the two protocols for this sample are all reliable. For the older sample LC-190 (**Fig. 6f**), D_e plateaus consistent with the expected D_e value (and the MET-pIRIR D_e plateau in **Figs. 6d** and **6e**) have also been reached in the D_e (T, t) plots. The D_e plateau for the pIRIR (50, 290) protocol begins at $t = 225$ s ($T = 290°C$), suggesting that the pIRIR$_{290}$ $D_{e\text{-is}}$ (the open circle at $t = 200$ s) for the method is underestimated due to fading effect. The pIRIR$_{290}$ $D_{e\text{-is}}$ is also underestimated within the error limits compared with the expected D_e. Hence, **Fig. 6f** indicates that in pIRIR (50, 290) protocol, using

the later integral of the pIRIR$_{290}$ can give more reliable D_e for the old sample LC-190. In contrast, the pIRIR$_{290}$ $D_{e\text{-is}}$ (the open diamond at $t = 200$ s) for the pIRIR (200, 290) method lies within the D_e plateau, and thus gives consistent D_e with the expected value. This agrees with the suggestion of Li and Li (2011b) that higher temperature first-step IR stimulation can better eliminate the fading signals in the two-step pIRIR dating for older samples. The results shown in **Fig. 6c** and f indicate the D_e (T, t) plot provides an effective judge for the two-step pIRIR protocols, and it can be used as an important criterion for the selection of appropriate measurement conditions.

Similar as in **Fig. 6**, for all samples in **Table 1**, D_e plateaus consistent with the expected D_e values can be identified in the D_e (T, t) plots of the four protocols. In **Fig. 7**, D_e (T, t) plots for samples in **Table 1** (except for sample LC-004 to avoid the non-bleachable dose effect), obtained using the four pIRIR methods (**Table 2**), are summarized. The plateau area and non-plateau area are shown as red and blue in colour, respectively, using the criteria that the D_e is consistent with plateau value within 1 σ standard error. The results show that D_e plateau reaches later for older samples for all the methods (simi-
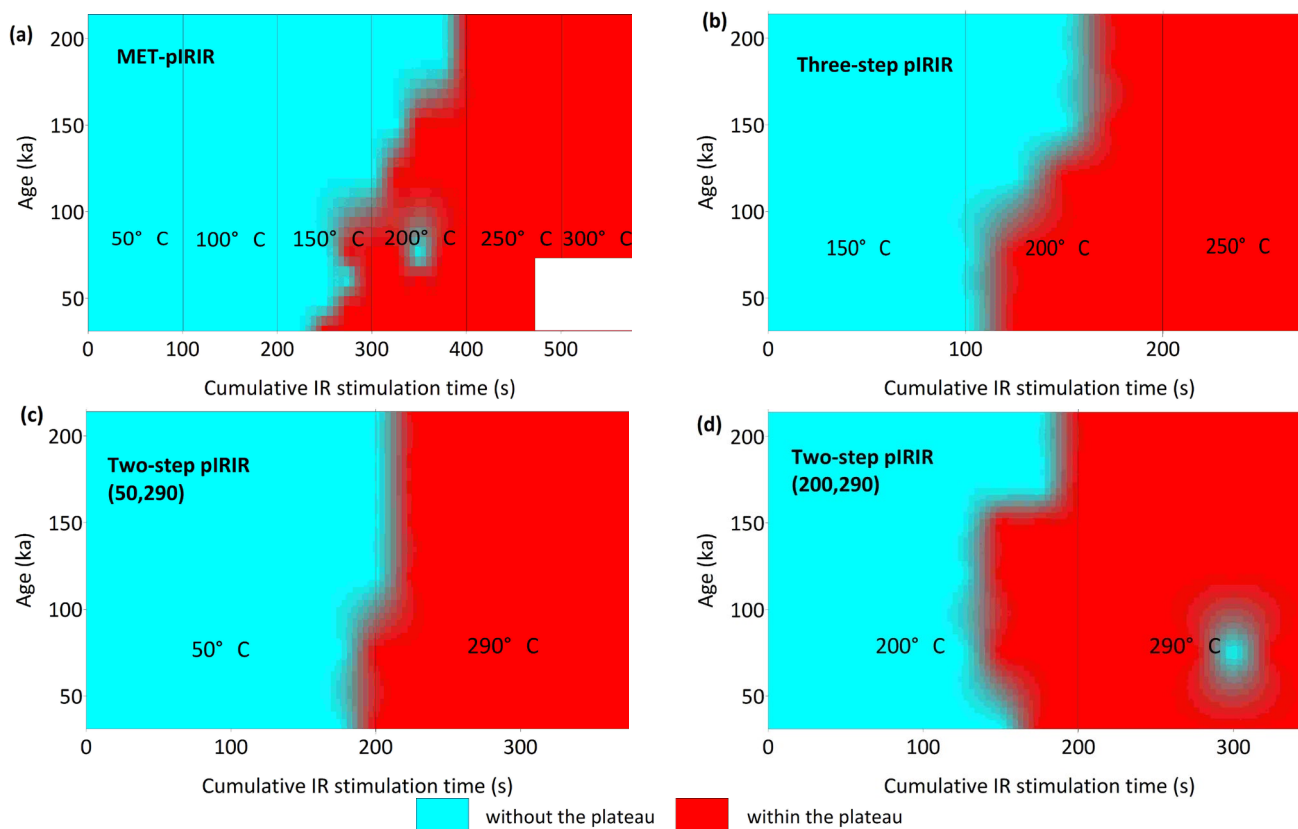
Fig. 7. *A summary of the* D_e *(T, t) for all the samples in Table 1 (except for LC-004), obtained using the pIRIR methods in Table 2: a) for the MET-pIRIR method; b) for the three-step pIRIR method; c) for the two-step pIRIR (50, 290) method and d) for the two-step pIRIR (200, 290) method. The red colour represents the plateau area and the blue colour represents the non-plateau area, using the criteria that the* D_e *is consistent with plateau value within 1 sigma standard error. In the MET-pIRIR dating results a), the highest T for samples younger than 75 ka was 250°C (with t up to 500 s), therefore data for T = 300°C (with t > 500 s) are absent.*

lar to **Fig. 5b**), suggesting that the effect of fading is related to the age of the sample. The D_e plateau can be used to judge which pIRIR $D_{e\text{-}is}$ gives more accurate dating result in these protocols for samples with different ages. In the MET-pIRIR method (**Fig. 7a**), for samples younger than ~100 ka, the MET-pIRIR $D_{e\text{-}is}$ of 200°C or above can be used for age determination; while for samples older than ~100 ka, MET-pIRIR $D_{e\text{-}is}$ obtained at 250 or 300°C are more reliable. In the three-step pIRIR protocol (**Fig. 7b**), the pIRIR$_{250}$ $D_{e\text{-}is}$ is reliable for all samples. The pIRIR$_{290}$ $D_{e\text{-}is}$ in the two-step pIRIR (50, 290) method (**Fig. 7c**) is valid for samples younger than ~100 ka. But for older samples, more accurate D_e value should be obtained from the later part of the pIRIR$_{290}$ signal. For the pIRIR (200, 290) method (**Fig. 7d**), all $D_{e\text{-}is}$ values obtained from the pIRIR$_{290}$ signal are considered to be reliable.

In summary, the results in **Figs. 6** and **7** indicate that the D_e plateau is a significant criterion for diagnosing the pIRIR dating results. This becomes especially important when independent age control is absent. The D_e (T, t) analysis is shown to be an effective tool for D_e plateau confirmation and detection for various pIRIR dating methods. It can be straightforwardly applied to dating results of different pIRIR protocols without additional measurement, and is applicable to individual aliquots. Hence, one can conveniently test it on already existed pIRIR data. In this study, the D_e (T, t) plot is only tested on Chinese loess samples. More tests of this method on samples with different sedimentary environment (e.g. non-aeolian sediments) should be done in further study.

6. CONCLUSION

In this study, a new self-diagnose method for the pIRIR dating protocols, the D_e (T, t) plot, was proposed, by combining the D_e (t) plots for the IRSL and pIRIR signals. The advantage of the D_e (T, t) plot is that it provides more data points when examining the pIRIR database, and it can be obtained directly from the single-aliquot dating results. The pattern of the D_e (T, t) plot is shown to be influenced by non-bleachable signal, partial bleaching and the anomalous fading effects. The achievement of a plateau in the D_e (T, t) plot is an indicator that the non-fading signal has been achieved, and the effects of non-bleachable dose and partial bleaching are negligible. Therefore, this plot can be served as a self-diagnose tool for the dating results. The D_e (T, t) analysis was applied to four pIRIR protocols, using aeolian samples from the Luochuan section with different ages. The results show that this self-diagnosing tool can be straightforwardly applied to these different pIRIR protocols, for judging the dating results and selecting appropriate measurement conditions.

REFERENCES

Aitken MJ, 1985. *Thermoluminescence Dating.* Academic Press .

Aitken MJ, 1998. *An introduction to luminescence dating.* Oxford University Press .

An ZS, Kukla GJ, Porter SC and Xiao JL, 1991. Magnetic susceptibility evidence of monsoon variation on the loess plateau of central China during the last 130,000 years. *Quaternary Research* 36(1): 29–36, DOI 10.1016/0033-5894(91)90015-W.

Auclair M, Lamothe M and Huot S, 2003. Measurement of anomalous fading for feldspar IRSL using SAR. *Radiation Measurements* 37(4–5): 487–492, DOI 10.1016/S1350-4487(03)00018-0.

Bailey RM, 2000. The interpretation of quartz optically stimulated luminescence equivalent dose versus time plots. *Radiation Measurements* 32(2): 129–140, DOI 10.1016/S1350-4487(99)00256-5.

Biswas RH, Williams MAJ, Raj R, Juyal N and Singhvi AK, 2013. Methodological studies on luminescence dating of volcanic ashes. *Quaternary Geochronology* 17: 14–25, DOI 10.1016/j.quageo.2013.03.004.

Buylaert JP, Jain M, Murray AS, Thomsen KJ, Thiel C and Sohbati R, 2012. A robust method for increasing the age range of feldspar IRSL dating. *Bor*eas 41(3): 435–451, DOI 10.1111/j.1502-3885.2012.00248.x.

Buylaert JP, Murray AS, Thomsen KJ and Jain M, 2009. Testing the potential of an elevated temperature IRSL signal from K-feldspar. *Radiation Measurements* 44(5–6): 560–565, DOI 10.1016/j.radmeas.2009.02.007.

Buylaert JP, Thiel C, Murray AS, Vandenberghe DAG, Yi S and Lu H, 2011. IRSL and post-IR IRSL residual doses recorded in modern dust samples from the Chinese Loess Plateau. *Geochronometria* 38(4): 432–440, DOI 10.2478/s13386-011-0047-0.

Ding ZL, Derbyshire E, Yang SL, Yu ZW, Xiong SF and Liu TS, 2002. Stacked 2.6-Ma grain size record from the Chinese loess based on five sections and correlation with the deep-sea delta O-18 record. *Paleoceanography* 17(3), DOI 10.1029/2001PA000725.

Fu X, Li B and Li SH, 2012a. Testing a multi-step post-IR IRSL dating method using polymineral fine grains from Chinese loess. *Quaternary Geochronology* 10: 8–15, DOI 10.1016/j.quageo.2011.12.004.

Fu X and Li SH, 2013. A modified multi-elevated-temperature post-IR IRSL protocol for dating Holocene sediments using K-feldspar. *Quaternary Geochronology* 17: 44–54, DOI 10.1016/j.quageo.2013.02.004.

Fu X, Zhang JF and Zhou LP, 2012b. Comparison of the properties of various optically stimulated luminescence signals from potassium feldspar. *Radiation Measurements* 47(3): 210–218, DOI 10.1016/j.radmeas.2011.12.007.

Huntley DJ, Godfrey-Smith DI and Thewalt MLW, 1985. Optical dating of sediments. *Nature* 313: 105–107, DOI 10.1038/313105a0.

Huntley DJ and Hancock RGV, 2001. The Rb content of K-feldspar grains being measured in optical dating. *Ancient TL* 19: 43–46.

Imbrie J, Haye JD, Martinson DB, McIntyre A, Mix AC, Morley JJ, Pisias NG, Prell WL and Shackleton NJ, 1984. The orbital theory of pleistocene climate: support from a revised chronology of the marine δ18O record. In: Berger A, Imbrie J, Hays G, Kukla G, Saltzman B (Eds.), *Milankovitch and Climate*. Reidel, Dordrecht, pp. 269–305.

Kars RH, Busschers FS and Wallinga J, 2012. Validating post IR-IRSL dating on K-feldspars through comparison with quartz OSL ages. *Quaternary Geochronology* 12: 74–86, DOI 10.1016/j.quageo.2012.05.001.

Lai ZP, 2010. Chronology and the upper dating limit for loess samples from Luochuan section in the Chinese Loess Plateau using quartz OSL SAR protocol. *Journal of Asian Earth Sciences* 37(2): 176–185, DOI 10.1016/j.jseaes.2009.08.003.

Li B and Li SH, 2011a. Luminescence dating of K-feldspar from sediments: A protocol without anomalous fading correction. *Quaternary Geochronology* 6(5): 468–479, DOI 10.1016/j.quageo.2011.05.001.

Li B and Li SH, 2011b. A reply to the comments by Thomsen *et al.* on "Luminescence dating of K-feldspar from sediments: a protocol without anomalous fading correction". *Quaternary Geochronology* 8: 49–51, DOI 10.1016/j.quageo.2011.10.001.

Li B and Li SH, 2012. Luminescence dating of Chinese loess beyond 130 ka using the non-fading signal from K-feldspar. *Quaternary Geochronology* 10: 24–31, DOI 10.1016/j.quageo.2011.12.005.

Li B, Roberts RG and Jacobs Z, 2013. On the dose dependency of the bleachable and non-bleachable components of IRSL from K-feldspar: Improved procedures for luminescence dating of Quaternary sediments. *Quaternary Geochronology* 17: 1–13, DOI 10.1016/j.quageo.2013.03.006.

Liu TS , 1985. *Loess and the Environment*. China Ocean Press.

Lowick S, Trauerstein M and Preusser F, 2012. Testing the application of post IR-IRSL dating to fine grain waterlain sediments. *Quaternary Geochronology* 8: 33–40, DOI 10.1016/j.quageo.2011.12.003.

Lu YC, Wang XL and Wintle AG, 2007. A new OSL chronology for dust accumulation in the last 130,000 yr for the Chinese Loess Plateau. *Quaternary Research* 67(1): 152–160, DOI 10.1016/j.yqres.2006.08.003.

Madsen AT, Buylaert JP and Murray AS, 2011. Luminescence dating of young coastal deposits from New Zealand using feldspar. *Geochronometria* 38(4): 378–390, DOI 10.2478/s13386-011-0042-5.

Porter SC and An ZS, 1995. Correlation between climate events in the North Atlantic and China during the last glaciation. *Nature* 375: 305–308, DOI 10.1038/375305a0.

Prescott JR and Hutton JT, 1994. Cosmic ray contributions to dose rates for luminescence and ESR dating: large depths and long-term time variations. *Radiation Measurements* 23(2–3): 497–500, DOI 10.1016/1350-4487(94)90086-8.

Qin JT and Zhou LP, 2012. Effects of thermally transferred signals in the post-IR IRSL SAR protocol. *Radiation Measurements* 47(9): 710–715, DOI 10.1016/j.radmeas.2011.12.011.

Reimann T, Tsukamoto S, Naumann M and Frechen M, 2011. The potential of using feldspars for optical dating of young coastal sediments-a test case from DarssZingst peninsula. *Quaternary Geochronology* 6(2): 207–222, DOI 10.1016/j.quageo.2010.10.001.

Reimann T and Tsukamoto S, 2012. Dating the recent past (<500 years) by post-IR IRSL feldspar -Examples from the North Sea and Baltic Sea coast. *Quaternary Geochronology* 10: 180–187, DOI 10.1016/j.quageo.2012.04.011.

Roberts HM, 2012. Testing Post-IR IRSL protocols for minimising fading in feldspars, using Alaskan loess with independent chronological control. *Radiation Measurements* 47(9): 716–724, DOI 10.1016/j.radmeas.2012.03.022.

Spooner NA, 1994. The anomalous fading of infrared-stimulated luminescence from feldspars. *Radiation Measurements* 23(2–3): 625–632, DOI 10.1016/1350-4487(94)90111-2.

Stevens T, Markovic SB, Zech M, Hambach U and Sümegi P, 2011. Dust deposition and climate in the Carpathian Basin over an independently dated last glacial-interglacial cycle. *Quaternary Science Reviews* 30(5–6): 662–681, DOI 10.1016/j.quascirev.2010.12.011.

Thiel C, Buylaert JP, Murray AS, Terhorst B, Hofer I, Tsukamoto S and Frechen M, 2011. Luminescence dating of the Stratzing loess profile (Austria) - testing the potential of an elevated temperature post-IR IRSL protocol. *Quaternary International* 234(1–2): 23–31, DOI 10.1016/j.quaint.2010.05.018.

Thomsen KJ, Murray AS, Jain M and Bøtter-Jensen L, 2008. Laboratory fading rates of various luminescence signals from feldspar-rich sediment extracts. *Radiation Measurements* 43(9–10): 1474–1486, DOI 10.1016/j.radmeas.2008.06.002.

Tsukamoto S, Denby PM, Murray AS and Bøtter-Jensen L, 2006. Time-resolved luminescence from feldspars: New insight into fading. *Radiation Measurements* 41(7–8): 790–795: DOI 10.1016/j.radmeas.2006.05.013.

Wallinga J, Murray A and Duller G, 2000. Underestimation of equivalent dose in single-aliquot optical dating of feldspars caused by preheating. *Radiation Measurements* 32(5–6): 691–695, DOI 10.1016/S1350-4487(00)00127-X.

Wang XL and Wintle AG, 2013. Investigating the contribution of recuperated TL to post-IR IRSL signals in a perthitic feldspar. *Radiation Measurements* 49: 82–87, DOI 10.1016/j.radmeas.2012.12.003.

Wintle AG, 1973. Anomalous fading of thermoluminescence in mineral samples. *Nature* 245: 143–144, DOI 10.1038/245143a0.

Zhao H and Li SH, 2005. Internal dose rate to K-feldspar grains from radioactive elements other than potassium. *Radiation Measurements* 40(1): 84–93, DOI 10.1016/j.radmeas.2004.11.004.

Zhu RX, Zhang R, Deng CL, Pan YX, Liu QS and Sun YB, 2007. Are Chinese loess deposits essentially continuous? *Geophysical Research Letters* 34(17): L17306, DOI 10.1029/2007GL030591.